A Model of Silicon Carbide Chemical Vapor Deposition

From analyses of the flatband potential, determined from the capacitance-voltage characteristics, it was confirmed that in the PSL electrodes, surface states pin the Fermi level. It was also demonstrated that the Pt deposition onto the PSL surface is very useful for a photoelectrochemical activation of the PSL, particularly in the thin PSL case.

Acknowledgments

The authors would like to thank Professor Y. Kiuchi and Professor S. Yoshida for their encouragement.

Manuscript received June 20, 1990.

Tokyo University of Agriculture and Technology assisted in meeting the publication costs of this article.

REFERENCES

1. N. Koshida, M. Nagasu, T. Sakusabe, and Y. Kiuchi, *This Journal*, **132**, 346 (1985).
2. N. Koshida and Y. Kiuchi, *Jpn. J. Appl. Phys.*, **24**, L166 (1985).
3. N. Koshida, H. Koyama, and Y. Kiuchi, *ibid.*, **25**, 1069 (1986).
4. N. Koshida, M. Nagasu, K. Echizenya, and Y. Kiuchi, *This Journal*, **133**, 2283 (1986).
5. M. Tomkiewicz, *ibid.*, **126**, 2220 (1979).
6. M. Tomkiewicz, *J. Photochemistry*, **29**, 165 (1985).
7. Y. Arita and Y. Sunohara, *This Journal*, **124**, 285 (1977).
8. T. Unagami and M. Seki, *ibid.*, **125**, 1339 (1978).
9. G. Bomchil, R. Herino, K. Barla, and J. C. Pfister, *ibid.*, **130**, 1611 (1983).
10. K. Barla, G. Bomchil, R. Herino, J. C. Pfister, and J. Baruchel, *J. Cryst. Growth*, **68**, 721 (1984).
11. K. Barla, R. Herino, G. Bomchil, J. C. Pfister, and A. Freund, *ibid.*, **68**, 727 (1984).
12. M. I. J. Beale, N. G. Chew, M. J. Uren, A. G. Cullis, and J. D. Benjamin, *Appl. Phys. Lett.*, **46**, 86 (1985).
13. I. M. Young, M. I. J. Beale, and J. D. Benjamin, *ibid.*, **46**, 1133 (1985).
14. M. I. J. Beale, J. D. Benjamin, M. J. Uren, N. G. Chew, and A. G. Cullis, *J. Cryst. Growth*, **73**, 622 (1985).
15. R. De Levie, in "Advances in Electrochemistry and Electrochemical Engineering," Vol. 6, P. Delahay, Editor, pp. 329-397, Interscience Publishers, Inc., New York (1967).
16. R. De Levie, *Electrochim. Acta*, **8**, 751 (1963).
17. R. De Levie, *ibid.*, **9**, 1231 (1964).

A Model of Silicon Carbide Chemical Vapor Deposition

Mark D. Allendorf* and Robert J. Kee

Sandia National Laboratories, Combustion Research Facility, Livermore, California 94551-0969

ABSTRACT

We present a model describing the interacting gas phase and surface chemistry present during the steady-state chemical vapor deposition (CVD) of silicon carbide (SiC). In this work, we treat the case of steady-state deposition of SiC from silane (SiH_4) and propane (C_3H_8) mixtures in hydrogen carrier gas at one atmosphere pressure. Epitaxial deposition is assumed to occur on a pre-existing epitaxial silicon carbide crystal. Pyrolysis of SiH_4 and C_3H_8 is modeled by 83 elementary gas-phase reactions. A set of 36 reactions of gas-phase species with the surface is used to simulate the deposition process. Rates for the gas/surface reactions were obtained from experimental measurements of sticking coefficients in the literature and theoretical estimates. Our results represent the first simulation of a silicon carbide deposition process that includes detailed descriptions of both the gas phase and surface reactions. The chemical reaction mechanism is also combined with a model of a rotating disk reactor (RDR), which is a convenient way to study the interaction of chemical reactions with fluid mechanics. Transport of species from the gas to the surface is accounted for using multicomponent transport properties. Predictions of deposition rates as a function of susceptor temperature, disk rotation rate, and reactant partial pressure are presented. In addition, velocity, temperature, and concentration profiles normal to the heated disk for 41 gas-phase species are determined using reactor conditions typical of epitaxial silicon carbide deposition on silicon substrates.

The resistance of silicon carbide (SiC) to high temperatures and corrosive chemical atmospheres makes it an attractive material for a variety of applications. For example, in applications requiring high-power or high-frequency, silicon carbide is useful as a semiconductor because of its large bandgap, high thermal conductivity, and other desirable characteristics (1). In its polycrystalline form, silicon carbide has potential for wear-, oxidation-, and high-temperature-resistant coatings; it can also be used as a diffusion barrier to prevent escape of fission products from the surface of fuel particles used in high-temperature gas-cooled reactors (2, 3). Silicon carbide can be formed from gas-phase reactants by an equally large variety of processes, including epitaxial deposition to produce thin films (1, 4-10), chemical vapor infiltration (CVI) of porous substrates (11), coating of substrate particles in fluidized bed reactors (2, 3), and gas-phase nucleation of ceramic powders (12). Chemical reactions occurring in both the gas phase and on heated surfaces are significant components of all these processes. The chemistry of the deposition process has been examined by several investigators through the calculation of gas- and solid-phase equilibria (13-16). Stinespring and Wormhoudt have also studied the kinetics of gas-phase silane (SiH_4) and propane (C_3H_8) decomposition, shedding considerable light upon the deposition process and pointing out the importance of gas-phase chemistry to the generation of reactive species (14). So far, however, no mechanism of silicon-carbide deposition has been proposed that simultaneously includes the critical effects of surface reactions as well as gas-phase chemistry.

In this work, we examine the case of steady-state deposition of SiC from SiH_4 and C_3H_8 mixtures in hydrogen carrier gas at one atmosphere pressure. This system was chosen for our study since a substantial body of experimental and theoretical data exists on which a detailed reaction mechanism can be based. In addition, due to recent work by Nishino (4-6), Davis (1, 7), and others (8-10), considerable progress has been made in improving chemical vapor deposition (CVD) techniques for growing electronics-grade single-crystal films of cubic (β) silicon carbide on silicon, renewing interest in this process from both experimental (1, 17) and theoretical (1, 14) points of view. The section on Chemical Reaction Mechanism describes chemical reactions for both the gas-phase decomposition of the reactants and the deposition of silicon carbide by collisions of gas-phase molecules with the surface. Silicon carbide is assumed to deposit epitaxially on a pre-existing epitaxial silicon carbide crystal. This mechanism is based on previous work we have done in the area of epitaxial silicon CVD and on results of experimental studies of silicon-carbide CVD in the literature. The mechanism and the results of the model presented here do not apply to the formation of the buffer layer during the temperature ramp phase of silicon carbide deposition on silicon substrates. Film

*Electrochemical Society Active Member.

growth during this phase is probably dominated by defects (7) which are not considered here.

We have also combined the reaction mechanism with the model of a rotating disk reactor (RDR) developed by Coltrin *et al.* (18) to predict deposition rates as a function of surface temperature, reactant partial pressure, and disk rotation rate. The RDR provides a convenient way to study the interaction of fluid mechanics and chemistry, since the Navier-Stokes equations (which are the equations of motion for a viscous, compressible fluid) can be reduced to a one-dimensional form by a mathematical transformation (19). Rotating disk reactors are also attractive from a practical viewpoint, since the temperature gradients and fluxes of gas-phase species normal to the disk are constant across the disk under some conditions (20, 21). The RDR thus has the potential to produce uniform deposition across the substrate, which can eliminate uneven deposition and unusual surface variations (such as swirl patterns on the deposit) caused by fluid convective effects found in barrel and channel reactors (10). The section on Mathematical Formulation discusses the mathematical details of the model and the numerical solution technique. Velocity, temperature, and concentration profiles normal to the heated surface for 41 gas-phase species are determined using reactor conditions typical of epitaxial silicon carbide deposition on silicon substrates. These results are presented in the section on Model Predictions and are limited to cases in which the reactant gases enter the reactor at room temperature, as occurs in cold wall reactors. The section on Comparisons with the Literature compares the predictions of our reaction mechanism with some of the experimental studies available in the literature.

Chemical Reaction Mechanism

At atmospheric pressure, at which most SiC deposition processes operate, considerable heat transfer occurs from the hot deposition surface to the gas. The residence time of the reactant gases at high temperature is sufficiently long that substantial decomposition of the reactants takes place. This produces a large number of decomposition products that collide and react with the surface to produce SiC. The surface reactivity of these products varies widely. Thus, an understanding of the details of the gas-phase chemical kinetics is critical to the accurate prediction of deposition rates. Fortunately, the gas-phase reactions that decompose SiH_4 and C_3H_8 are well understood, so that estimation of their rates is not required. Very little is known of the kinetics of reactions at the surface, however, requiring that several simplifying assumptions be made in order to proceed. Following a brief presentation of the gas-phase pyrolysis mechanisms, details of which are relatively straightforward, we present an in-depth discussion of the surface reaction mechanism.

Gas-phase chemistry.—The reactions used to model the gas-phase pyrolysis of silane and propane are shown in Table I. All reactions in the gas phase are reversible; the reverse rates are calculated from thermochemical data. No adjustment of gas-phase reaction rates was performed to match experimental SiC deposition rate data in the literature.

The mechanism for the thermal decomposition of silane was obtained from Ref. (18) (Table I). The rate constant for the unimolecular decomposition of silane (reaction [I-58]) quoted in that reference was obtained by fitting RRKM results at 600, 800, and 1000 K. Since silicon carbide deposition processes typically operate at temperatures much higher than this, we use rate constants obtained by fitting RRKM results at 600, 1150, and 1750 K (22). The rates of all other reactions are the same as in Ref. (18).

The elementary reactions occurring during hydrocarbon pyrolysis (Table I) were obtained from two sources. Reactions [I-25]-[I-57] are from Miller *et al.* (23). The remaining reactions are taken from a paper by Westbrook and Pitz (24). Reactions involving species with four or more carbon atoms have been eliminated from the mechanism, as have C_2H and C, since our calculations show that their concentrations are very small at the temperatures of interest. Thus, they do not make a significant contribution to the deposition rate. In addition, reactions involving species with silicon-carbon bonds have not been included in the mechanism since Stinespring and Wormhoudt conclude that these species do not contribute significantly to the deposition rate, based on their calculations of the gas-phase reaction kinetics (14). A similar conclusion is reached based on results of equilibrium calculations (13).

Surface reactions.—In this model, collision and subsequent reaction of gas-phase molecules with the heated surface are responsible for SiC deposition (and not formation of gas-phase Si-C species, as discussed above). Thus, surface reaction chemistry is a critical component of any model of SiC deposition. Tables II and III list the surface species and surface reactions employed in our mechanism of SiC deposition. Unlike the gas-phase decomposition reactions, thermodynamic and kinetic data for these species and reactions are only now becoming available. This paucity of data requires several simplifying assumptions that we now discuss.

In the mechanism we have assumed that deposition occurs at dangling bond sites on the silicon-carbide surface. The number of these sites is estimated from the density of silicon carbide ($6.52 \times 10^{14}/cm^2$), and this number is conserved in the model. Gas-phase species that collide with the surface and stick to such sites are considered as "surface species;" surface species that are covered by subsequent reaction with additional gas-phase species are converted to bulk silicon carbide. To obtain the correct stoichiometry (one silicon for every carbon deposited) we have written the surface reactions so that carbon species deposit only on sites occupied by silicon, Si(s), and silicon deposits only on sites occupied by carbon, C(s). This restriction clearly does not permit formation of either pure silicon or carbon phases; however, experiments (6, 16, 28) indicate that only SiC is formed when the C/Si ratio is ≤ 1.00. Note that, although there is no bulk species defined as "SiC," silicon carbide is deposited with the correct density by depositing bulk silicon, Si(b), and bulk carbon, C(b), with effective densities determined by their mass fraction in silicon carbide.

Experimental evidence for the existence of the surface species listed in Table II is very limited, although electron energy loss spectroscopy (EELS) indicates that SiH_2 can be adsorbed on the silicon surface (29, 30). The species $SiH_2(s)$ (silylene adsorbed on the surface) is not strictly required by our model, since H_2 could be immediately desorbed from the surface (for example, reaction [III-21] could be written $SiH_2 + C(s) \rightarrow Si(s) + C(b) + H_2$.) However, Buss *et al.* have obtained a rate constant for H_2 desorption from silicon using molecular beam methods (32), so we have incorporated this result into our model. SiH(s) and CH(s) were included so that molecules with odd numbers of hydrogen atoms can stick to the surface without desorbing hydrogen atoms. Since there is no evidence that hydrogen atoms can desorb (at least in this temperature range) from a silicon or silicon-carbide surface, these atoms must remain on the surface until they can recombine with another hydrogen atom to desorb as H_2. This is a more realistic treatment of the surface chemistry since reactions involving gas-phase species with odd numbers of hydrogen atoms have the same order with respect to surface sites as do reactions of species with even numbers of hydrogen atoms. For example, reaction [23] in Table III could have been written $2SiH_3 + 2SiC(s) \rightarrow 2Si(s) + 3H_2(s) + 2SiC(b)$, but this is second-order in both surface sites and reactant. Similarly, the use of (Si)H and C(H) surface species permits H atoms, which are known to stick to silicon surfaces with unit probability (31), to reside on the surface.

In formulating a reaction mechanism for surface deposition we have chosen to write the gas-surface reactions as irreversible surface adsorptions, the rates of which are (with a few exceptions) determined by reactive sticking coefficients. Irreversibility was assumed because the lack of accurate thermochemical data for surface species does not permit calculation of reverse reaction rates from the equilibrium and forward rate constants. This effectively eliminates two processes, etching of the surface by hydrogen and sublimation of silicon, since we have chosen not

Table I. Gas-phase reactions
Reaction mechanism rate coefficients in form $k_f = AT^{\beta} \exp(-E/RT)$
Units are moles, cubic centimeters, seconds, Kelvins, and calories/mole

Reaction	A	β	E
1. $C_3H_8 \leftrightarrow CH_3 + C_2H_5$	1 698E + 16	0 0	84840.0
2. $CH_4 + C_3H_8 \leftrightarrow CH_4 + i^*C_3H_7$	1.097E + 15	0.0	25140.0
3. $CH_3 + C_3H_8 \leftrightarrow CH_4 + n^*C_3H_7$	1 097E + 15	0.0	25140.0
4. $H + C_3H_8 \leftrightarrow H_2 + i^*C_3H_7$	8 710E + 06	2.0	5000.0
5. $H + C_3H_8 \leftrightarrow H_2 + n^*C_3H_7$	5.623E + 07	2.0	7700 0
6. $i^*C_3H_7 \leftrightarrow H + C_3H_6$	6.310E + 13	0 0	36900 0
7. $i^*C_3H_7 \leftrightarrow CH_3 + C_2H_4$	1.995E + 10	0 0	29500 0
8. $n^*C_3H_7 \leftrightarrow H + C_3H_6$	1.259E + 14	0 0	37000.0
9. $n^*C_3H_7 \leftrightarrow CH_3 + C_2H_4$	9.550E + 13	0.0	31000.0
10. $i^*C_3H_7 + C_3H_8 \leftrightarrow n^*C_3H_7 + C_3H_8$	3.020E + 10	0.0	12900.0
11 $C_2H_3 + C_3H_8 \leftrightarrow C_2H_4 + i^*C_3H_7$	1.000E + 11	0.0	10400.0
12. $C_2H_3 + C_3H_8 \leftrightarrow C_2H_4 + n^*C_3H_7$	1.000E + 11	0.0	10400 0
13. $C_2H_5 + C_3H_8 \leftrightarrow C_2H_6 + i^*C_3H_7$	1.000E + 11	0.0	10400.0
14. $C_2H_5 + C_3H_8 \leftrightarrow C_2H_6 + n^*C_3H_7$	1.000E + 11	0.0	10400.0
15. $C_3H_6 + H \leftrightarrow CH_2CHCH_2 + H_2$	5.010E + 12	0.0	1500.0
16. $C_3H_6 + CH_3 \leftrightarrow CH_2CHCH_2 + CH_4$	8.910E + 10	0.0	8500.0
17. $C_3H_6 + C_2H_5 \leftrightarrow CH_2CHCH_2 + C_2H_6$	1.000E + 11	0.0	9200.0
18. $C_3H_8 + CH_2CHCH_2 \leftrightarrow i^*C_3H_7 + C_3H_6$	3.980E + 11	0.0	16200.0
19. $C_3H_8 + CH_2CHCH_2 \leftrightarrow n^*C_3H_7 + C_3H_6$	3.980E + 11	0.0	16200.0
20. $CH_2CHCH_2 \leftrightarrow C_3H_4 + H$	3.980E + 13	0.0	70000 0
21 $C_3H_6 \leftrightarrow CH_2CHCH_2 + H$	1.000E + 13	0.0	78000.0
22. $C_3H_6 \leftrightarrow C_2H_3 + CH_3$	6 310E + 15	0.0	85800.0
23. $CH_2CHCH_2 + H \leftrightarrow C_3H_4 + H_2$	1.000E + 13	0.0	0.0
24. $CH_2CHCH_2 + CH_3 \leftrightarrow C_3H_4 + CH_4$	1.000E + 12	0.0	0.0
25. $CH_3 + CH_3(+M) \leftrightarrow C_2H_6(+M)$			
High pressure limit:	9.03E + 16	−1 18	654 0
Low pressure limit:	3 18E + 41	−7.03	2762.0
Troe parameters:[a] α = 0.6041, T^* = 6927, T^{**} = 132			
Enhanced third-body efficiencies: H_2 = 2			
26. $CH_3 + H(+M) \leftrightarrow CH_4(+M)$			
High pressure limit:	6.00E + 16	−1 0	0.0
Low pressure limit:	8.00E + 26	−3.0	0.0
SRI parameters:[b] 0.45, 797.0, 979, 1.0			
Enhanced third-body efficiencies: H_2 = 2			
27. $CH_4 + H \leftrightarrow CH_3 + H_2$	2.20E + 04	3.0	8750.0
28. $CH_3 + H \leftrightarrow {}^3CH_2 + H_2$	9.00E + 13	0 0	15100.0
29. $^3CH_2 + H \leftrightarrow CH + H_2$	1.00E + 18	−1.560	0.0
30. $CH + C_2H \leftrightarrow C_3H_2 + H$	1.00E + 14	0.0	0.0
31. $CH + CH_2 \leftrightarrow C_2H_2 + H$	4.00E + 13	0.0	0.0
32. $CH + CH_3 \leftrightarrow C_2H_3 + H$	3.00E + 13	0.0	0.0
33. $CH + CH_4 \leftrightarrow C_2H_4 + H$	6.00E + 13	0.0	0.0
34. $C_2H_6 + CH_3 \leftrightarrow C_2H_5 + CH_4$	5.50E + 00	4 000	8300.0
35. $C_2H_6 + H \leftrightarrow C_2H_5 + H_2$	5.40E + 02	3 500	5210.0
36. $C_2H_4 + H \leftrightarrow C_2H_3 + H_2$	1.10E + 14	0 0	8500.0
37. $^3CH_2 + CH_3 \leftrightarrow C_2H_4 + H$	3.00E + 13	0.0	0.0
38. $H + C_2H_4(+M) \leftrightarrow C_2H_5(+M)$			
High pressure limit:	2 21E + 13	0.0	2066.0
Low pressure limit:	6.37E + 27	−2.76	−54.0
Enhanced third-body efficiencies: H_2 = 2 0			
39. $C_2H_5 + H \leftrightarrow CH_3 + CH_3$	1 00E + 14	0.0	0.0
40. $H_2 + C_2H \leftrightarrow C_2H_2 + H$	4.09E + 05	2.390	864.3
41. $H + C_2H_2(+M) \leftrightarrow C_2H_3(+M)$			
High presure limit:	5.54E + 12	0.0	2410.0
Low pressure limit:	2.67E + 27	−3.5	2410.0
Enhanced third-body efficiencies: H_2 = 2.0			
42. $C_2H_3 + H \leftrightarrow C_2H_2 + H_2$	4.00E + 13	0 0	0.0
43. $C_2H_3 + C_2H \leftrightarrow C_2H_2 + C_2H_2$	3.00E + 13	0.0	0.0
44. $C_2H_3 + CH \leftrightarrow CH_2 + C_2H_2$	5.00E + 13	0.0	0.0
45. $^1CH_2 + M \leftrightarrow {}^3CH_2 + M$	1.00E + 13	0.0	0.0
Enhanced third-body efficiencies: H = 0.0			
46. $^1CH_2 + CH_4 \leftrightarrow CH_3 + CH_3$	4.00E + 13	0.0	0.0
47. $^1CH_2 + C_2H_6 \leftrightarrow CH_3 + C_2H_5$	1.20E + 14	0.0	0.0
48. $^1CH_2 + H_2 \leftrightarrow CH_3 + H$	7.00E + 13	0 0	0.0
49 $^1CH_2 + H \leftrightarrow CH_2 + H$	2.00E + 14	0 0	0.0
50. $CH_2 + CH_2 \leftrightarrow C_2H_2 + H + H$	4.00E + 13	0 0	0.0
51. $CH_2 + C_2H_2 \leftrightarrow H_2CCCH + H$	1.20E + 13	0.0	6600 0
52. $^1CH_2 + C_2H_2 \leftrightarrow H_2CCCH + H$	3.00E + 13	0 0	0.0
53. $C_2H_2 + M \leftrightarrow C_2H + H + M$	4.20E + 16	0.0	107000.0
54. $C_2H_4 + M \leftrightarrow C_2H_2 + H_2 + M$	1.50E + 15	0.0	55800 0
55. $C_2H_4 + M \leftrightarrow C_2H_3 + H + M$	1.40E + 16	0.0	82360 0
56. $H + H + M \leftrightarrow H_2 + M$	1.00E + 18	−1.000	0 0
Enhanced third-body efficiencies: H_2 = 0.0			
57. $H + H + H_2 \leftrightarrow H_2 + H_2$	9 200E + 16	-0 6	0.0
58. $SiH_4 \leftrightarrow SiH_2 + H_2$	6.671E + 29	−4.795	63450.0
59. $SiH_4 \leftrightarrow SiH_3 + H$	3.690E + 15	0.0	93000.0
60. $Si_2H_6 \leftrightarrow SiH_4 + SiH_2$	3.240E + 29	-4.240	58000 0
61. $SiH_4 + H \leftrightarrow SiH_3 + H_2$	1.460E + 13	0.0	2500.0
62. $SiH_4 + SiH_3 \leftrightarrow Si_2H_5 + H_2$	1.770E + 12	0 0	4400.0
63. $SiH_4 + SiH \leftrightarrow Si_2H_3 + H_2$	1.450E + 12	0.0	2000.0
64 $SiH_4 + SiH \leftrightarrow Si_2H_5$	1 430E + 13	0.0	2000.0
65. $SiH_2 \leftrightarrow Si + H_2$	1.060E + 14	−0.880	45000.0
66. $SiH_2 + H \leftrightarrow SiH + H_2$	1.390E + 13	0.0	2000.0
67 $SiH_2 + H \leftrightarrow SiH_3$	3.810E + 13	0.0	2000.0
68. $SiH_2 + SiH_3 \leftrightarrow Si_2H_5$	6.580E + 12	0.0	2000.0
69. $SiH_2 + Si_2 \leftrightarrow Si_3 + H_2$	3.550E + 11	0.0	2000 0
70. $SiH_2 + Si_3 \leftrightarrow Si_3H_2 + Si_2$	1.430E + 11	0.0	16200.0
71. $H_2SiSiH_2 \leftrightarrow Si_2H_2 + H_2$	3.160E + 14	0.0	53000 0
72. $Si_2H_6 \leftrightarrow H_3SiSiH + H_2$	7.940E + 15	0.0	56400.0
73. $H_2 + SiH \leftrightarrow SiH_3$	3.450E + 13	0.0	2000.0
74. $H_2 + Si_2 \leftrightarrow Si_2H_2$	1.540E + 13	0.0	2000.0
75. $H_2 + Si_2 \leftrightarrow SiH + SiH$	1.540E + 13	0.0	40000 0
76. $H_2 + Si_3 \leftrightarrow Si + Si_2H_2$	9.790E + 12	0 0	47200.0
77. $Si_2H_5 \leftrightarrow Si_2H_3 + H_2$	3 160E + 14	0 0	53000 0
78. $Si_2H_2 + H \leftrightarrow Si_2H_3$	8.630E + 14	0.0	2000.0
79. $H + Si_2 \leftrightarrow SiH + Si$	5.150E + 13	0 0	5300 0
80. $H_3SiSiH + SiH_4 \leftrightarrow Si_3H_8$	6 020E + 13	0.0	0.0
81. $SiH_2 + Si_2H_6 \leftrightarrow Si_3H_8$	1 810E + 14	0.0	0 0
82. $SiH_3 + Si_2H_5 \leftrightarrow Si_3H_8$	3.310E + 13	0.0	0 0
83. $H_3SiSiH \leftrightarrow H_2SiSiH_2$	1 150E + 20	−3.060	6630.0

[a]Fall-off reaction in the Troe form: $F_{cent}(T) = (1 - \alpha) \exp(-T/T^*) + \alpha \exp(-T^{**}/T)$ [see Ref. (52)].
[b]Fall-off reaction in the SRI form [see Ref (52)].

Table II. Surface species

Si(s)	A silicon surface site
C(s)	A carbon surface site
SiH_2(s)	An SiH_2 group adsorbed on the silicon carbide surface
SiH(s)	An SiH group adsorbed on the silicon carbide surface
CH(s)	A CH group adsorbed on the silicon carbide surface
(C)H	Hydrogen atom adsorbed on a carbon surface site
(Si)H	Hydrogen atom adsorbed on a silicon surface site
Si(b)	Bulk silicon deposited at the density of silicon carbide
C(b)	Bulk carbon deposited at the density of silicon carbide

to include these as explicit irreversible reactions. As will be seen below, however, etching is not expected to be significant at the temperatures of interest here. In addition, although surface graphitization attributed to silicon sublimation is observed when SiC is heated to temperatures above 1300 K (33), the surfaces of CVD-SiC films are not believed to be carbon rich.

This approach has been used successfully to model deposition of both gallium arsenide (25) and silicon from silane (18). Although some reactions in the mechanism are more global in nature than those likely to be occurring on the surface (for example, reaction [III-16] is third-order in Si(s) sites), evidence from surface experiments indicates that the reactions in Table III are a reasonable representation of the important processes. Studies of ethylene adsorption on silicon using EELS (26, 27) indicate that hydrocarbons irreversibly adsorb with release of molecular hydrogen. At temperatures above 1000 K, only silicon carbide is observed on the surface; vibrational bands associated with C—C and Si—H bonds found at lower temperatures disappear. This indicates that the details of individual reactions occurring on the surface during silicon carbide formation are probably not critical to a successful model, since they are rapid and the product is always the same, viz., every collision that results in a molecule sticking to the surface causes an atom (or atoms) of silicon or carbon to be deposited. The surface chemistry problem is greatly simplified by this since it reduces the number of reactions in the mechanism.

Sticking coefficients are converted to Arrhenius form by multiplying each coefficient by the rate of gas-phase collisions with the surface (derived from kinetic theory), then equating this quantity with the mass action expression for the specific reaction. This yields a rate constant of the form $AT^{1/2}$. We assume that sticking coefficients obtained on silicon surfaces are applicable to silicon carbide, since very few have been measured on silicon-carbide surfaces. This probably has little effect as far as reactions of radicals with the surface is concerned; it is not unreasonable to assume that these relatively unstable species will react on surfaces with high efficiency to produce much more stable adsorbates. Our predictions regarding silicon deposition should thus be essentially unaffected also, since our calculations show (see the section on Model Predictions) that silicon-containing radicals are primarily responsible for silicon deposition. Sticking coefficients for two important hydrocarbon species, C_2H_4 and C_2H_2, were derived from measurements of adsorption on a silicon substrate. Since a silicon carbide monolayer forms immediately, however, the sticking coefficient is effectively measured on silicon carbide. Thus, carbon deposition should also not be seriously affected by assuming an equivalence between the silicon and silicon-carbide surfaces.

Experimentally determined sticking coefficients are available for several important silicon species in the mechanism. Data for silane are from Ref. (34) and were obtained from studies in a CVD reactor using hydrogen carrier gas at pressures approaching one atmosphere. As in Ref. (18), we have assumed that the sticking coefficient for disilane is ten times that of silane. The sticking coefficient of SiH_2 on a hydrogenated silicon-carbon surface has been measured by resonance-enhanced multiphoton ionization techniques to be 0.15 at 300 K and >0.5 for vibrationally excited SiH_2 (35). Computational studies (36) of SiH_2 adsorption on Si(111) (7 × 7) [the high-temperature modification of the Si(111) surface] are in general agreement with these results, yielding sticking coefficients near unity. Based on these studies we use a sticking coefficient of 1.00 for SiH_2. The results of theory also indicate that SiH_2 decomposes by desorbing a hydrogen molecule and

Table III. Surface reactions

Reaction mechanism rate coefficients in form $k_f = AT^{\beta} \exp(-E/RT)$
Units are moles, cubic centimeters, seconds, Kelvins, and calories/mole

Reaction	A	β	E
1. H + Si(s) → (Si)H + Si(b)	2.180E + 12	0.5	0.0
2. H + C(s) → (C)H + C(b)	2.180E + 12	0.5	0.0
3. 2(Si)H + 2Si(b) → 2Si(s) + H_2	7.230E + 24	0.0	61000.0
4. 2(C)H + 2C(b) → 2C(s) + H_2	7.230E + 24	0.0	61000.0
5. CH_4 + Si(s) → C(s) + Si(b) + $2H_2$	4.197E + 07	0.5	0.0
6. CH_3 + Si(s) → CH(s) + Si(b) + H_2	8.666E + 11	0.5	0.0
7. CH_2 + Si(s) → C(s) + Si(b) + H_2	8.972E + 11	0.5	0.0
8. CH_2(s) + Si(s) → C(s) + Si(b) + H_2	8.972E + 11	0.5	0.0
9. CH + Si(s) → CH(s) + Si(b)	9.310E + 11	0.5	0.0
10. C_2H_5 + 2Si(s) → C(s) + CH(s) + $2H_2$ + 2Si(b)	5.760E + 20	0.5	0.0
11. C_2H_4 + 2Si(s) → 2C(s) + $2H_2$ + 2Si(b)	9.367E + 17	0.5	0.0
12. C_2H_3 + 2Si(s) → C(s) + CH(s) + 2Si(b) + H_2	5.970E + 20	0.5	0.0
13. C_2H_2 + 2Si(s) → 2C(s) + 2Si(b) + H_2	1.216E + 19	0.5	0.0
14. i*C_3H_7 + 3Si(s) → 2C(s) + CH(s) + 3Si(b) + $3H_2$	4.360E + 29	0.5	0.0
15. n*C_3H_7 + 3Si(s) → 2C(s) + CH(s) + $3H_2$ + 3Si(b)	4.360E + 29	0.5	0.0
16. C_3H_6 + 3Si(s) → 3C(s) + $3H_2$ + 3Si(b)	7.061E + 26	0.5	0.0
17. C_3H_4 + 3Si(s) → 3C(s) + 3Si(b) + $2H_2$	4.524E + 29	0.5	0.0
18. H_2CCCH + 3Si(s) → 2C(s) + CH(s) + H_2 + 3Si(b)	4.580E + 29	0.5	0.0
19. CH_2CHCH_2 + 3Si(s) → 2C(s) + CH(s) + $2H_2$ + 3Si(b)	4.470E + 29	0.5	0.0
20. C_3H_2 + 3Si(s) → 3C(s) + H_2 + 3Si(b)	4.642E + 29	0.5	0.0
21. SiH_2 + C(s) → C(b) + SiH_2(s)	6.120E + 11	0.5	0.0
22. SiH_4 + C(s) → C(b) + SiH_2(s) + H_2	3.184E + 10	0.5	18678.0
23. SiH_3 + C(s) → C(b) + SiH(s) + H_2	6.026E + 11	0.5	0.0
24. SiH + C(s) → C(b) + SiH(s)	6.227E + 11	0.5	0.0
25. Si + C(s) → C(b) + Si(s)	6.334E + 11	0.5	0.0
26. Si_2H_5 + 2C(s) → 2C(b) + SiH(s) + SiH_2(s) + H_2	3.950E + 20	0.5	0.0
27. Si_2H_3 + 2C(s) → 2C(b) + SiH_2(s) + SiH(s)	4.023E + 20	0.5	0.0
28. Si_2 + 2C(s) → 2C(b) + 2Si(s)	4.140E + 20	0.5	0.0
29. Si_2H_6 + 2C(s) → 2Si(s) + 2C(b) + $3H_2$	2.113E + 20	0.5	18678.0
30. H_3SiSiH + 2C(s) → 2C(b) + $2SiH_2$(s)	3.999E + 20	0.5	0.0
31. H_2SiSiH_2 + 2C(s) → 2C(b) + $2SiH_2$(s)	3.999E + 20	0.5	0.0
32. Si_2H_2 + 2C(s) → 2C(b) + 2SiH(s)	4.070E + 20	0.5	0.0
33. Si_3 + 3C(s) → 3C(b) + 3Si(s)	2.302E + 29	0.5	0.0
34. 2CH(s) → 2C(s) + H_2	2.250E + 24	0.0	61000.0
35. 2SiH(s) → 2Si(s) + H_2	2.250E + 24	0.0	61000.0
36. SiH_2(s) → Si(s) + H_2	2.912E + 14	0.0	9000.0

not by dissociating to give two H atoms adsorbed on the surface (36); this finding has been incorporated in our model as reaction [III-36]. Finally, the sticking coefficient of SiH adsorption on amorphous hydrogenated silicon has been measured using a laser-induced fluorescence technique (37); a value of 0.94 was found and is used here.

In the absence of experimental data, we use sticking coefficients determined by computational studies. A classical trajectory study of silicon atoms interacting with the Si(100) surface found a value of 0.965 at 1500 K for the sticking coefficient (38); this value was found to be independent of temperature. We use a value of 1.00 at all temperatures for the silicon-atom sticking coefficient. For all other silicon-containing species, we assume unity sticking coefficients.

Investigations using ultrahigh vacuum surface techniques have also yielded reactive sticking coefficient data for the three most important hydrocarbon species for silicon-carbide deposition. Again, data were obtained on Si(111) and Si(100) surfaces and not on silicon carbide itself; we assume these surfaces are equivalent. The results of Bozso *et al.* (39) and Stinespring and Wormhoudt (17) are in good agreement on the sticking coefficient for C_2H_4; we use the value of 1.6×10^{-3} (measured over the temperature range 1062-1227 K) from (17). In an early study, Mogab and Leamy obtained a sticking coefficient for acetylene of 0.02-0.03 over the temperature range 1073-1373 K (40); we use 0.02. Stinespring and Wormhoudt also measured sticking coefficients for methane and propane and obtained values of 5.0×10^{-5} and 2.0×10^{-5}, respectively (17). We assume that the initial hydrocarbon reactant, propane, does not stick to the surface; at the temperatures typical of SiC deposition (1500-1800 K), propane is not a significant component of the gas phase near the surface, so this produces little error while eliminating a reaction that is third-order in silicon surface sites. The reactive sticking coefficient of propene (C_3H_6) is assumed to be the same as that of C_2H_4; Bozack *et al.* (41) propose that C_3H_6 and C_2H_4 form similar adsorbates on the silicon surface.

All hydrocarbon radical species are assumed to stick with unit efficiency. Although there are no experimental measurements of hydrocarbon radical sticking coefficients or theoretical results available, enhanced reactivity of propene with a hydrogenated-Si(100) surface is thought to be caused by formation of a C_3H_7 radical on the surface (42). It is thus reasonable to assume that hydrocarbon radicals have a higher probability of reacting with the surface than stable molecules.

Data obtained from experiments and theory indicate that hydrogen molecules do not stick to silicon surfaces (31) or do so only at high temperatures (43). Based on these results, we assume that hydrogen molecules do not stick to the silicon carbide surface. Hydrogen has been shown to etch silicon carbide at very high temperatures (>1800 K) (44, 45), so our model will probably overpredict the deposition rate at these temperatures. Since current techniques typically use silicon substrates (which melt at 1683 K) for making electronics-grade silicon carbide, substrate temperatures usually do not exceed 1650 K. Hydrogen etch rates are low at these temperatures (44), so it is reasonable to ignore them. Nevertheless, we include some results for surface temperatures above 1800 K to clarify points regarding the mechanism.

Hydrogen atoms are a significant component of the gas phase at these temperatures; they are found to stick with unit efficiency to silicon surfaces (31) and to inactivate the surface to adsorption of hydrocarbons by capping dangling bonds (41). It is thus important to account for their surface reactivity. Since we are not aware of any evidence for inactivation of silicon-carbide surfaces due to hydrogen atom accumulation, we assume that surface diffusion of H-atoms is sufficiently rapid at these temperatures that they can recombine and desorb as hydrogen molecules. There is evidence in the literature to support this view. Laser desorption studies by Koehler *et al.* of hydrogen atoms on Si(111) at high coverages indicate that recombination of hydrogen atoms occurs on the surface followed by desorption of H_2; second-order kinetics are obeyed and an activation energy of 61 kcal/mole is measured (46). Surface diffusion of hydrogen atoms was not observed below 740 K and could also not be seen above that temperature, due to desorption of molecular hydrogen. Although Koehler *et al.* conclude that hydrogen atoms have low mobility at temperatures below 1300 K (the surface temperature achieved during the laser pulse), indicating that a large energy barrier to diffusion exists, the laser desorption data are also consistent with a diffusion activation barrier that is comparable to that for recombination of H-atoms on neighboring sites. Theoretical estimates of H-atom diffusion constants on silicon surfaces have activation barriers of around 63 kcal/mole (47), in agreement with this result. Additional evidence that hydrogen atoms do not accumulate on the silicon-carbide surface comes from the EELS studies of C_2H_4 on Si(111) referred to earlier (26, 27). At temperatures below 1000 K a vibrational band characteristic of the Si—H bond is observed, indicating that hydrogen atoms are adsorbed on the surface. At higher temperatures, however, this band disappears, showing that the Si—H bond has been broken. No evidence for Si—H bonds is observed above 1000 K, indicating that hydrogen has been desorbed. The rate for hydrogen atom recombination (Reactions [III-3] and [III-4]) used in these studies is that obtained from the thermal desorption studies (46).

In the absence of experimental data, we assume that the CH(s) and SiH(s) species also diffuse rapidly. We use the same rate coefficient for their recombination as for hydrogen atom recombination, except that we have scaled the A-factor by $\nu^{1/2}$, where ν is the vibrational frequency of the adsorbed species, assuming that the A-factor is proportional to the vibrational frequency (48). A similar activation energy for the two processes is expected in light of the comparable Si—H and Si—C bond strengths (49). Classical trajectory studies of silicon atoms diffusing on silicon (38) and experimental estimates (50) yield large diffusion coefficients for atomic silicon at temperatures typical of SiC CVD ($>10^{-4}$ cm^2/s at 1500 K). It thus seems reasonable to assume that radical species also diffuse rapidly across the growing silicon carbide surface at high temperatures.

The results of the analysis of existing experimental and theoretical data in this section may be summarized as follows. Reactions of stable gas-phase species with the surface are two-five orders of magnitude less rapid than are those of unstable radical or unsaturated species. The latter are assumed to have unity sticking coefficients, an assumption which is confirmed by experimental data obtained for several silicon-containing radicals. Sticking coefficients of stable hydrocarbons do not change substantially with temperature, justifying our derivation of the rate constant based on kinetic theory. Although data are not available for all species used in the mechanism, sufficient information has been obtained to make reasonable generalizations regarding the rates of gas/surface reactions.

Mathematical Formulation

Under certain circumstances the flow in the vicinity of a rotating disk can (by mathematical transformation) be described as an ordinary differential-equation boundary-value problem. The transformation that reduces the full three-dimensional fluid transport equations (19) was first described in 1921 by von Karman for an infinite-radius disk spinning in an isothermal, quiescent, semi-infinite environment. In this geometry, scalar quantities depend only on the distance from the disk and not on radial or angular position; thus, the mass and energy fluxes to the surface are uniform everywhere. Recent investigations (18, 25, 51) have extended the von Karman analysis to include complex chemical kinetics and are capable of predicting deposition chemistry. Thus, an infinite-radius disk provides an especially convenient geometry in which to study the interaction of complex gas-phase and surface chemistry with the gas-phase transport of species.

The boundary value problem that we solve (25) is stated as

Mixture continuity

$$\frac{du}{dx} + 2V + \frac{u}{\rho}\frac{d\rho}{dx} = 0 \qquad [1]$$

Radial momentum

$$\frac{d}{dx}\left(\mu\frac{dV}{dx}\right) - \rho u\frac{dV}{dx} - \rho(V^2 - W^2) = 0 \quad [2]$$

Circumferential momentum

$$\frac{d}{dx}\left(\mu\frac{dW}{dx}\right) - \rho u\frac{dW}{dx} - 2\rho VW = 0 \quad [3]$$

Thermal energy

$$\frac{d}{dx}\left(\lambda\frac{dT}{dx}\right) - \rho c_p u\frac{dT}{dx} - \sum_{k=1}^{K_g}\left(c_{pk}\rho Y_k V_k\frac{dT}{dx} + \omega_k h_k\right) = 0 \quad [4]$$

Gas-phase species continuity

$$\frac{d\rho Y_k V_k}{dx} + \rho u\frac{dY_k}{dx} - M_k\dot{\omega}_k = 0 \quad (k = 1, K_g) \quad [5]$$

Equation of state

$$P = \frac{\rho RT}{\bar{M}} \quad [6]$$

In the governing system of equations, the independent variable is x, the height above the disk. The dependent variables are: temperature T, the axial velocity u, the radial velocity variable (normalized by the radius) $V = v/r$, the circumferential velocity variable (normalized by the radius) $W = w/r$, the gas-phase species mass fractions Y_k, and the surface species site fractions Z_k. Variables in the equations include the mass density ρ, the viscosity μ, the thermal conductivity λ, the constant-pressure heat capacity c_p, the species diffusion velocities V_k, the species enthalpies h_k; the molecular weights are specified by the M_k. The chemical production rates of gas-phase species by gas-phase reactions (52) are given by $\dot{\omega}_k$. There are K_s "surface" species and K_g gas-phase species.

In a steady-state problem the net production rate of species (including gas-phase, surface, or bulk species) by surface reactions is time independent

$$\dot{s}_k = 0\ (k = 1, K_s) \quad [7]$$

Note that Eq. [7] applies only to the "surface" species and not to the bulk species. In physical terms, this expression states that at steady state (no time dependence) the surface composition remains constant; *i.e.*, even though surface species are being created and destroyed by surface reactions, they are being created and destroyed at the same rate. The chemical production rates of gas-phase species by surface reaction are balanced by the diffusive and convective fluxes to and away from the surface. This point is discussed further in a subsequent section on boundary conditions. The rate of production of the bulk-phase species is a measure of the film growth rate. Equation [7] therefore, must be included with Eq. [1]-[6] in the system of governing equations, although it can be thought of as a (very complex) boundary condition on the gas-phase system of equations. Note the distinction between $\dot{\omega}_k$, which is the production of gas-phase species by gas-phase reactions, and $\dot{s}_k$ which is the production of species (possibly including gas-phase species) by heterogeneous reactions at the surface. $\dot{s}_k$ is a function of the gas-phase composition immediately above the surface, the surface composition, and the bulk-material composition.

We use a multicomponent transport formulation (53, 54) in which the species diffusion velocities are expressed as

$$V_k = \frac{1}{X_k\bar{M}}\sum_{j=1}^{K_g} M_j D_{kj}\frac{dX_j}{dx} - \frac{D_k^T}{\rho Y_k}\frac{1}{T}\frac{dT}{dx} \quad [8]$$

where X_k are the mole fractions and D_{kj} and D_k^T are the ordinary multicomponent diffusion coefficient matrix and the thermal diffusion (Soret effect) coefficient.

Surface chemistry.—The mass rate of consumption or creation of species by heterogeneous reaction at the surface, $\dot{s}_k$, is given by

$$\dot{s}_k = M_k\sum_{i=1}^{I_s}(\nu''_{ki} - \nu'_{ki})q_i \quad [9]$$

where q_i is the rate of progress for each of the I_s surface reactions, and ν_{ki} are the stoichiometric coefficients for the surface reactions. Each surface reaction proceeds according to the law of mass action, where the rate of progress of reaction i is

$$q_i = k_{f_i}\prod_{k=1}^{K}[X_k]^{\nu'_{ik}} - k_{r_i}\prod_{k=1}^{K}[X_k]^{\nu''_{ik}} \quad [10]$$

$$[X_k] = \begin{cases} Y_k\rho/M_k \text{ gas (mol/cm}^3\text{)} \\ Z_k\Gamma \text{ surface (mol/cm}^2\text{)} \\ a_k \text{ bulk (unitless)} \end{cases} \quad [11]$$

The concentrations $[X_k]$ for the gas-phase species are the molar concentrations. In our surface-reaction formalism we distinguish between "surface" species that form the top-most layer of the solid (in contact with the gas) and the bulk-phase solid. The surface species' concentration is given in terms of the fraction Z_k of available sites occupied by each species and the surface site density is given by Γ (mol/cm^2). The bulk species "concentration" is described by an activity a_k. The rate constants k_i are taken in the usual, modified-Arrhenius form.

Boundary conditions.—The gas-phase mass flux, j_k, of each species at the surface is balanced by the creation or depletion rate of that species by surface reaction: $j_k = \dot{s}_k$. The gas-phase mass flux at the surface is a combination of diffusive and convective processes and is expressed as: $j_k = \rho Y_k u - \rho Y_k V_k$, where the mass-averaged (Stefan) velocity at the surface is computed from the surface reaction rates summed over all the gas-phase species

$$u = \sum_{k=1}^{K_g}\frac{\dot{s}_k}{\rho} \quad [12]$$

At the disk surface we must also specify boundary conditions for the temperature and the radial and circumferential velocities. In the simulations here, we will prescribe a fixed disk temperature. The surface velocities are specified by a no-slip condition as $V = 0$ and $W = \Omega$, where Ω is the disk rotation rate (radians/s).

Far from the disk surface, the boundary conditions require that the temperature and species concentrations be prescribed at reactor inlet values; in this case, an unreacted mixture of silane, propane, and carrier gas at room temperature. Furthermore, we assume that the radial and circumferential velocities are zero. In deriving the system of governing equations it is assumed that the radial pressure gradient is zero. A consequence of this is that there can be no prescribed axial velocity at the reactor inlet. The spinning disk simply acts as a pump that draws fluid into the reactor and the inlet velocity is determined as a part of the solution. Evans and Greif (21) developed an extension to the system of equations that allows the inlet axial velocity to be specified as a boundary condition. However, for all of the calculations in this paper we use the usual rotating-disk equations (no imposed flow) and the asymptotic axial velocity is part of the solution.

Numerical solution technique.—The governing differential equations are discretized via finite differences on a mesh network that spans the gas-phase region above the disk. While the problem is formally posed on a semi-infinite domain, we solve it on a fixed domain that is sufficiently large to represent the semi-infinite behavior. In the problems presented here, the domain extends 2.0-3.0 cm above the disk surface, depending on the temperature chosen for the disk. The method of numerical solution has been presented in detail elsewhere (18, 25, 55, 56). Briefly, we solve the system of algebraic equations that results from the finite-difference discretization by a damped mod-

ified Newton algorithm. The mesh network is adjusted adaptively to place mesh points in a way that represents the solution accurately, yet uses a minimum number of points. The first step in any iterative solution procedure is to guess a trial solution. When the Newton algorithm fails to converge, the solution estimate is conditioned by a period of time integration on the associated time-dependent problem (55, 56). The Newton method converges very rapidly (quadratically) when it has a trial estimate to the solution that is sufficiently close to the actual solution. Unfortunately, for a problem as complex as this one, it is nearly impossible to guess a solution that is within the domain of convergence for Newton's method. While Newton's method may fail when the initial iterate is far from the solution, solving the time-dependent problem by implicit numerical methods is usually stable, even for higher nonlinear and stiff problems. In fact, carrying the time integration out to the steady solution is one method of determining the solution we seek. However, the asymptotic convergence to the steady state is very slow compared to a successful Newton iteration. Therefore, we only carry the transient solution far enough to ensure success by the Newton iteration.

Model Predictions

In a typical steady-state silicon-carbide CVD process, propane and silane in a mole ratio Si/C $\leq$ 1.0 are mixed with hydrogen carrier gas at atmospheric pressure. Susceptor temperatures for deposition on silicon are in the 1600-1680 K range, below the melting point of silicon. We have adopted a set of conditions as a "base case" that are typical of steady-state silicon carbide CVD processes reported in the literature (5, 6, 10). Input mole fractions of silane and propane are 6.0×10^{-4} and 2.0×10^{-4}, respectively, (mole ratio Si/C = 1.00) in hydrogen carrier gas at one atmosphere total reactor pressure. For the base case the disk (susceptor) temperature is 1625 K.

An appropriate range of disk spin rates must also be chosen. Since the RDR model does not include the fluid mechanical effects of buoyancy, disk rotation rates must be sufficiently large that the convective forces generated by the rotating disk are large compared with buoyancy forces. A real RDR operating under conditions where this is not the case would contain fluid mechanical instabilities (gas recirculation patterns), which usually cause uneven deposition. At high susceptor temperatures, such as those examined here, buoyancy effects can be quite large. Evans and Greif define a mixed convection parameter (20) for the RDR, $Gr/Re^{3/2}$, where Gr is the Grashof number, $g(1 - \rho_w)$ $r_d^3/\rho_w \nu_\infty^2$, and Re is the Reynold's number, $r_d^2\Omega/\nu_\infty$ (g is the acceleration of gravity, ρ_w is a dimensionless density evaluated at the surface of the disk, r_d is the dimensionless radius of the disk, and ν_∞ is the kinematic viscosity at the inlet). When this parameter is of order unity, buoyancy effects can be neglected. Solutions of the Navier-Stokes equations and flow visualization experiments demonstrate that values of $Gr/Re^{3/2}$ less than about five produce flow conditions that correspond to the ideal one-dimensional flow over an infinite-radius disk (20, 57) simulated by the RDR model. For the temperature range considered in this study, disk rotation rates of 900 rpm or greater are required in order to maintain $Gr/Re^{3/2} \leq 5$; we chose 1200 rpm for the base case and examine the silicon carbide deposition over the 1200-2000 rpm range of disk rotation rates.

We now proceed with a detailed discussion of the model predictions for the base case. The fluid flow predictions of the RDR model are discussed in detail elsewhere (18); a limited discussion is presented here, however, since the temperatures examined are much higher than those studied previously. Figure 1 shows temperature and velocity profiles as a function of distance above the disk. The boundary layer is approximately 1.5 cm thick at this temperature and rotation rate; as discussed earlier, this layer becomes thinner as the spin rate increases, scaling as $\Omega^{1/2}$. The rotation of the disk creates convection which pulls gas toward it, producing an input gas velocity magnitude of about 8.5 cm/s at 1200 rpm and a disk temperature of 1625 K. Gas approaching the heated susceptor is first accelerated toward it by the decrease in gas density (due to the higher temperature) and then slowed down to near zero at the disk surface [as pointed out previously (18), the velocity at the surface is not exactly zero because of the deposition occurring there]. The profiles of the radial and circumferential velocity are similar in shape to those calculated in the earlier study of the RDR (18); these velocities increase linearly with the radial coordinate and thus the data shown in Fig. 1 are scaled by the value of r.

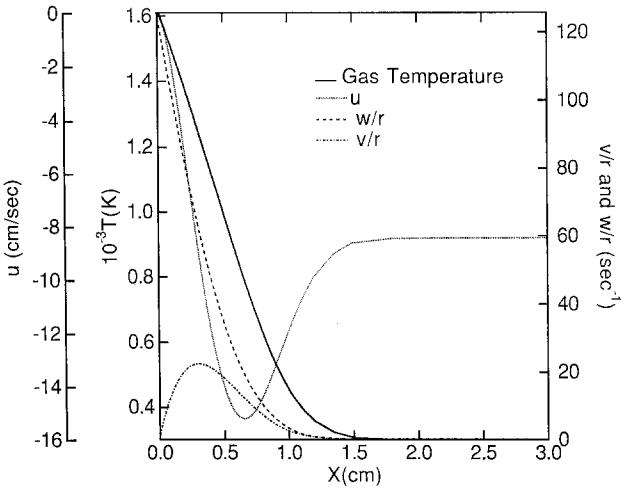

Fig. 1. Gas temperatures and velocities as a function of height above the rotating disk. Reactor conditions: disk temperature: 1625 K; mole fraction C_3H_8: 2.0×10^{-4}; mole fraction SiH_4: 6.0×10^{-4}; hydrogen carrier gas at 1 atm pressure. Input gas temperature: 300 K. Disk rotation rate: 1200 rpm.

Concentration profiles as a function of height above the disk are predicted by the model for the 41 gas-phase species used in the chemical reaction mechanism (concentration and temperature are independent of r and θ, so no profiles are given as a function of these parameters.) Figure 2 displays concentrations for the species most significant to the deposition; only the region close to the heated disk is shown as this is where most of the gas-phase decomposition occurs. These profiles show that the two reactants display very different behavior in this environment. The hydrocarbon reactant, propane, is more than 96% decomposed at a height of 2 mm above the disk (Fig. 2a), pyrolyzing to form primarily the stable products methane (CH_4), ethylene (C_2H_4), and acetylene (C_2H_2). Concentrations of all hydrocarbon radical species are at least two-orders of magnitude lower than the concentrations of these stable species. Comparison of our results with equilibrium calculations (14) shows that concentrations of C_2H_4 and C_2H_2 at the disk are higher than those expected at equilibrium. In addition, the concentration of C_2H_4 exceeds that of C_2H_2 by about a factor of ten, highlighting an important consequence of the difference in geometries between the RDR and channel or barrel reactors. At the low input flow velocities used in channel or barrel reactors (2.5 cm/s is typical), the process gases flow only about 1.0 cm downstream from the susceptor leading edge before the boundary layer fills the channel. Isotherms at the leading edge are thus nearly perpendicular to the gas flow, so that cold reactants encounter high temperatures at the upstream edge of the susceptor and are rapidly heated to the susceptor temperature, which in most cases exceeds 1600 K. Since the reactions that produce C_2H_4 are fast at temperatures as much as 300 K lower than this, substantial concentrations of C_2H_4 are quickly produced. As the gas continues to flow over the hot susceptor, the higher activation-energy process that converts C_2H_4 to C_2H_2 (reaction [I-54]) occurs at significant rates, decomposing most of the C_2H_4 to C_2H_2. This is reflected in the simulations of channel-reactor gas-phase kinetics performed by Stinespring and Wormhoudt (14) (at a susceptor temperature of 1665 K), in which the concentration of C_2H_2 near the susceptor exceeds that of C_2H_4 by about a factor of ten. Cold reactive gases in the RDR, however, have shorter residence times at the high

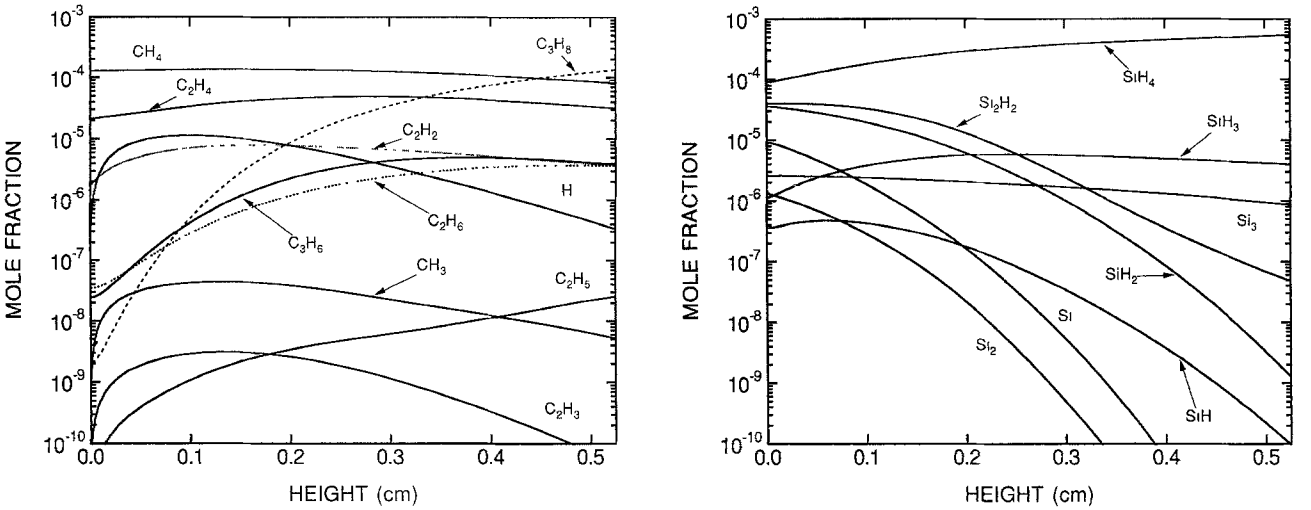

Fig. 2. Gas-phase mole-fraction profiles of significant hydrocarbon (a, left) and silicon (b, right) species for the reactor conditions in Fig. 1. For clarity, not all species used in the mechanism are shown.

temperatures required to decompose C_2H_4 to C_2H_2. Thus, at RDR susceptor temperatures comparable to those used by Stinespring and Wormhoudt, the concentration of C_2H_4 at the disk in the RDR exceeds that of C_2H_2. The reaction of C_2H_2 at the surface also contributes to its lower concentration in the gas phase near the surface; its larger sticking coefficient relative to C_2H_4 depletes the C_2H_2 concentration to a greater extent than does the reaction of C_2H_4 with the surface.

In contrast to propane, silane is only 52% decomposed at 2.0 mm and only ~85% decomposed at the disk surface (Fig. 2B). This is due to the strong inhibition of its unimolecular decomposition (reaction [I-58]) by the hydrogen carrier gas; the rate of reaction [I-58] peaks at the surface, where the temperature is highest. The decomposition leads primarily to reactive species such as SiH_2, Si, and Si_2H_2. Concentrations of all but one of the silicon-containing species are within a factor of three of the values expected for a purely gas-phase equilibrium (Si_3H_8 is within a factor of five). Larger deviations from equilibrium are observed at distances less than 2 mm above the surface, as surface reactions begin to affect the gas phase. These results are consistent with those of previous investigators (14, 59), who concluded that the reactions which follow [I-58] are sufficiently fast that the concentrations of silicon-containing species approach equilibrium in the absence of surface reactions. In contrast with earlier simulations of the gas-phase SiH_4/C_3H_8 kinetics (14), however, our mechanism predicts that SiH_4 remains the silicon species in highest concentration throughout the gas phase, rather than SiH_2. This is probably due to the higher activation energy we have used for reaction [I-58], which is based on the most recent heat of formation for SiH_2 (64.3 Kcal/mol) (18).

Figure 2 also shows that, for most species, steep concentration gradients into the disk do not exist. The only species whose concentrations are greatly reduced near the surface are hydrogen atoms and hydrocarbon radicals (such as CH_3 and C_2H_3). This shows that reactions of gas-phase species with the surface at 1625 K are not so fast that species concentrations near the disk are depleted, which would cause the deposition to become transport limited. The shape of these profiles is a direct consequence of the differing surface reactivities of the molecules in the gas phase. As noted above, most of the SiH_4 decomposes to unstable species that react efficiently with the surface. Propane decomposition, however, yields largely stable hydrocarbons, which react slowly with the surface compared with silicon species such as Si and SiH_2. This produces a low steady-state concentration of C(s) sites (<1% of the total sites) and a high concentration of Si(s) sites. Since, in our model, the deposition of silicon depends on the existence of C(s) sites, reactions of silicon species with the surface are limited by the slow surface chemistry of the stable hydrocarbons. Thus, the high gas-phase concentrations of stable hydrocarbons and their low surface reaction rates causes the rate-limiting step in SiC deposition to be the formation of C(s) sites.

In Fig. 3 the relative contributions of the principal species responsible for deposition are plotted as a function of temperature. Among the gas-phase silicon species, only SiH_2, Si, and SiH_3 contribute significantly to the deposition. The contribution of silane to the deposition rate is negligible; its sticking coefficient is only about 10^{-4} at these temperatures. Increasing the temperature causes the SiH_2 to decompose to silicon atoms, but deposition rates are not substantially affected by this because the sticking coefficients and transport rates of the two species are roughly the same. One consequence of our mechanism is that the species Si_2H_2, whose concentration slightly exceeds that of SiH_2, contributes little to the deposition. This is a result of our assumption that reaction [III-32] has a second-order dependence on C(s) surface sites. It has little effect on the deposition rate, however, since it is the reaction of hydrocarbons with the surface that limits the growth rate. The incorporation of carbon into the growing deposit is dominated by the stable hydrocarbons C_2H_4 and C_2H_2, with smaller contributions from CH_4, C_3H_4, and CH_3 (not shown in Fig. 3 for clarity.) Increasing the surface temperature changes the composition of the gas phase and thus the dominant depositing species from C_2H_4 to C_2H_2.

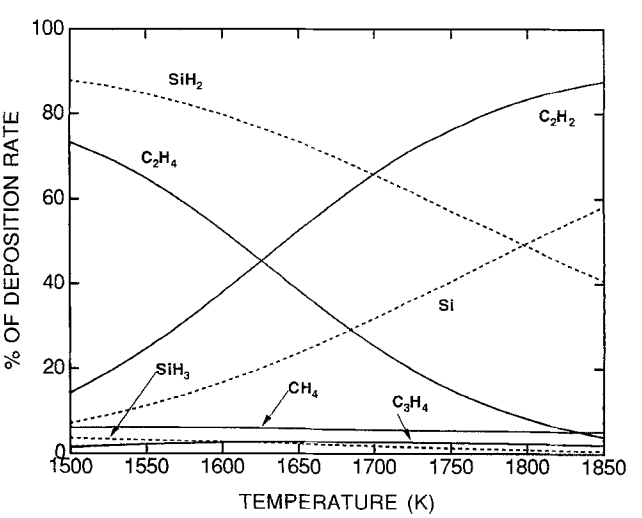

Fig. 3. Contribution of gas-phase species to the silicon carbide deposition rate as a function of disk temperature. Only the most significant contributing species are shown. Contributions are given as percentages of the total carbon and total silicon deposition rates. Reactor conditions are the same as in Fig. 1.

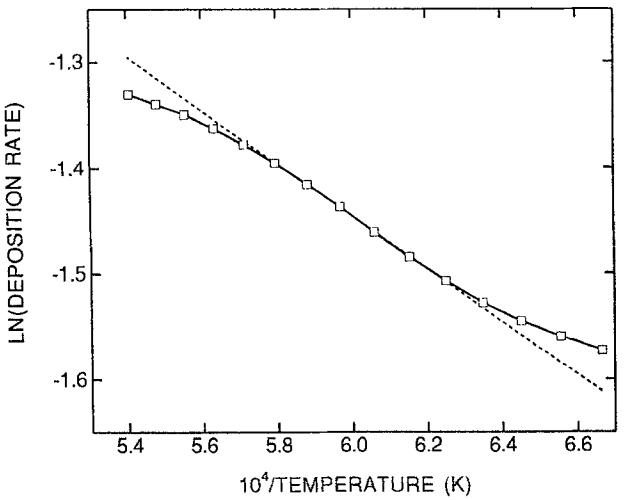

Fig. 4. Temperature dependence of the silicon carbide deposition rate. The dashed line is from a linear least squares fit to the 1600-1725 K data. Reactor conditions as in Fig. 1.

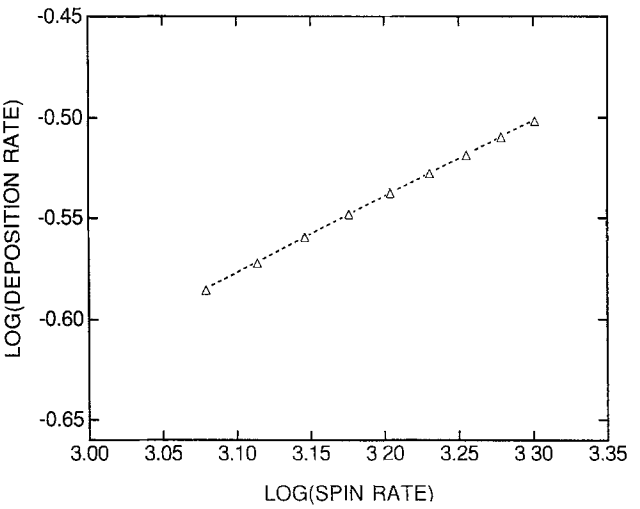

Fig. 5. Dependence of the silicon carbide deposition rate on risk rotation rate. Disk temperature: 1800 K. The dashed line is a linear least squares fit to the data, yielding a dependence of the deposition rate on disk rotation rate of $\Omega^{0.37}$. All other reactor conditions as in Fig. 1.

Deposition due to the species CH_4 and radical species is largely unaffected by this temperature change.

The temperature dependence of the deposition rate is shown in Fig. 4. For low surface temperatures (1500-1600 K) the deposition rate is weakly dependent on temperature. At higher surface temperatures, the growth rate increases more rapidly, following Arrhenius behavior; a small activation barrier of 4.9 Kcal/mol over the 1600-1725 K temperature range is obtained by fitting the data (dashed line, Fig. 4). Above 1725 K, the deposition rate tapers off with temperature. This complex dependence on surface temperature is understandable in terms of the relative concentrations of reactive hydrocarbons in the gas phase and their rates of reaction with the surface. At low surface temperatures, the weak temperature dependence of the growth rate is caused by the slow surface reaction rate of C_2H_4, which is the primary species responsible for carbon deposition (Fig. 3). Heating the surface to temperatures between 1600 and 1725 K causes the composition of the gas phase to change substantially as C_2H_4 is converted to C_2H_2 by reactions [I-36], [I-41], and [I-54]. Since C_2H_2 is adsorbed more efficiently by the surface than C_2H_4 (reacting 32 times faster with the surface than C_2H_4), it becomes the primary hydrocarbon responsible for carbon deposition above 1625 K. The 1600-1725 K temperature range thus represents a transition between the surface chemistries of C_2H_4 and C_2H_2. At the highest temperature examined (1850 K), nearly 85% of the deposited carbon comes from C_2H_2. Even at these high temperatures the rates of hydrocarbon surface reactions still limit the rate of deposition, as evidenced by concentration profiles at 1850 K showing substantial concentrations of C_2H_2 near the surface (not shown.) The saturation of the growth rate observed in Fig. 4 is thus not due to mass transport limitations caused by high surface reaction rates. Additional evidence of this is seen in the dependence of the deposition rate on disk rotation rate at 1800 K, which scales as $\Omega^{0.37}$ (Fig. 5) rather than as $\Omega^{0.50}$, as is expected in the transport-limited case.

The temperature dependence of the deposition rate can be understood in more quantitative terms by performing a sensitivity analysis, which determines the effect of individual reaction rates on gas-phase concentrations and the deposition rate. Such an analysis is helpful in determining which reactions in a complex mechanism are rate limiting. Sensitivity coefficients are defined as $\partial\varphi_i/\partial\alpha_k$, where φ_i is a component of the solution (such as the deposition rate or a gas-phase concentration at some location) and α_k is the Arrhenius "A-factor" for the kth reaction. These coefficients represent the fractional increase (or decrease, if the coefficient is negative) in the deposition rate that occurs when the rate of reaction k is doubled.

The sensitivity of the deposition rate to several gas-phase and surface reactions is shown in Table IV for four different temperatures (only the largest sensitivity coefficients are given). At the lowest disk temperature (1500 K), the growth rate is most sensitive to the rate of the C_2H_4 surface reaction (reaction [III-10]), with much smaller sensitivities to the other major depositing species and little or no sensitivity to gas-phase reactions. This confirms that deposition is surface reaction-limited in the low temperature (1500-1600 K) regime. Increasing the surface temperature to 1625 K decreases the sensitivity to reaction [III-10], consistent with the decreasing concentration of C_2H_4 near the disk. At high disk temperatures (above 1725 K) where the deposition rate no longer increases substantially with temperature, the deposition rate is virtually insensitive to the rates of both gas-phase and surface reactions; no sensitivity to the surface reaction contributing the most to the deposition rate (C_2H_2 adsorption, reaction [III-11]) is observed in spite of the fact that substantial concentrations of C_2H_2 are still present near the disk.

This behavior at high temperatures can be understood by examining the sensitivity of the gas-phase C_2H_2 concentration near the surface to reaction [I-54] (the reaction primarily responsible for C_2H_2 production) and to the C_2H_2 surface reaction (Table V). Consider an arbitrary point in the gas phase just above the surface. The rates of chemical reaction and mass diffusion at this point must be balanced since the model determines a steady-state solution. If, now, the surface reactivity of C_2H_2 is increased (by increasing the rate of reaction [III-11]), the flux of C_2H_2 to the surface will also increase. Since this causes the concentration of C_2H_2 near the surface to decrease, the rate of gas-phase C_2H_2 production must increase to balance the increased C_2H_2 flux. The sensitivities in Table V show that this is pos-

Table IV. Normalized deposition rate sensitivity coefficients

T_{DISK} (K)	[I-54]	[I-59]	[III-10]	[III-11]	[III-21]
1500	0.025	0.002	0.180	0.039	0.003
1625	0.054	0.011	0.091	0.013	0.001
1750	0.038	0.016	0.021	0.021	0.000
1850	0.017	0.016	0.004	0.025	0.000

Table V. Gas-phase C_2H_2 sensitivity coefficients evaluated at the surface

T_{DISK} (K)	[I-54]	[III-11]
1500	0.65	−1.00
1625	0.45	−1.00
1750	0.17	−1.00
1850	0.05	−1.00

sible at 1500 K; although doubling the rate of reaction [III-11] would decrease the concentration of C_2H_2 at the surface by a factor of two (sensitivity coefficient of −1.0 for reaction [III-11]), the production of C_2H_2 via reaction [I-54] can make up for most of the increased flux (positive sensitivity coefficient of 0.65 for [I-54]). At high temperatures (1750-1850 K), however, the sensitivity to reaction [I-54] is much smaller, showing that the C_2H_2 production rate cannot increase further due to the low concentration of C_2H_4. Thus, the effect of increasing the rate of reaction [III-11] is to decrease the concentration of C_2H_2 throughout the gas phase, so that no net increase in the flux of C_2H_2 to the surface can occur. This results in a deposition rate that is relatively independent of temperature above 1725 K.

Figures 6 and 7 plot the dependence of the deposition rate on the composition of the reactant gas stream. In Fig. 6, the deposition rate is plotted as a function of the silane concentration, holding the propane mole fraction constant, while Fig. 7 shows data for varying propane concentration with fixed silane concentration. As expected, the deposition rate is found to be independent of the silane concentration but depends linearly on the propane concentration (which extrapolates to zero for a propane mole fraction of zero.) Gas-phase decomposition of silane produces radical species that stick with unit efficiency to the surface of the growing film, so that silicon atoms are deposited as soon as a C(s) site becomes available. Propane decomposition, on the other hand, produces largely stable hydrocarbon species that react much more slowly with the surface. Since the growth mechanism is constrained so that a carbon site must be available in order for a silicon atom to be deposited, growth is limited by the rate at which surface carbon sites can be produced, resulting in a dependence on the input propane concentration.

Comparisons with the Literature

Although no experimental studies of silicon carbide CVD have been performed in an RDR, there have been numerous investigations of this process in cold wall channel and barrel reactors (for the sake of brevity, we will refer only to channel reactors). Unfortunately, direct comparisons of RDR simulations with results obtained in these reactors are difficult due to the large differences in geometry. In particular, the thermal and mass-transfer boundary layers in the RDR are constant across the disk, while those in channel reactors change as a function of position in the reactor. This causes deposition rates to vary across the surface, so that it is unclear at what location in a channel reactor the deposition rate should be comparable to those obtained in the RDR. Dimensional analysis to determine the functional dependence of the mass transport boundary layer thickness can be used as a rough guide for locating

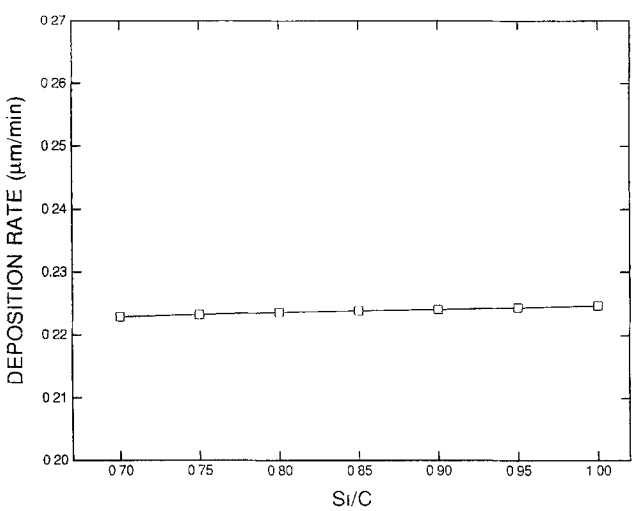

Fig. 6. Dependence of the silicon carbide deposition rate on the input mole fraction of SiH_4. For these calculations, the input mole fraction of C_3H_8 was held constant at 2.0×10^{-4} while the mole fraction of SiH_4 was changed. Reactor conditions as in Fig. 1.

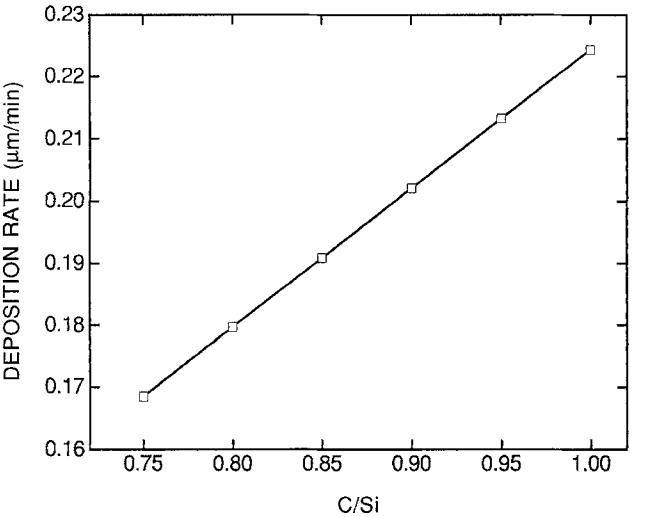

Fig. 7. Dependence of the silicon carbide deposition rate on the input mole fraction of C_3H_8. For these calculations, the input mole fraction of SiH_4 was held constant at 6.0×10^{-4} while the mole fraction of C_3H_8 was changed. Reactor conditions as in Fig. 1.

regions of comparable mass transport rate (and thus, comparable deposition rates.) In a channel reactor, the mass transport boundary layer thickness scales approximately as $(\nu x/u_{avg})^{1/2}$, while in the RDR it scales as $(\nu/\Omega)^{1/2}$, where ν is the kinematic viscosity, x is the distance downstream from the leading edge of the boundary layer (usually taken as the upstream edge of the susceptor) in a channel reactor, and u_{avg} is the velocity of the incoming gas (at 300 K) in the channel reactor. Combining these two relationships gives an inequality defining the portion of the boundary layer in a channel reactor whose thickness is comparable to that of the RDR for identical values of ν

$$x \leq u_{avg}/\Omega \qquad [15]$$

Using the base conditions for the RDR, we have Ω = 126 s^{-1} (1200 rpm); a typical value of u_{avg} found in the literature (10) is 2.5 cm/s. This yields $x \leq 0.02$ cm, showing that rates of mass transport (and, hence, deposition rates) in the two reactors are comparable only at the leading edge of the susceptor. At distances further downstream than 0.02 cm from the leading edge, the boundary layer will always be thicker in a channel reactor, so deposition rates are expected to be lower than those found in the RDR. Since deposition rates in a channel reactor are usually measured near the center of the susceptor, we expect that such rates reported in the literature will be significantly smaller than those found in the RDR. This is, in fact, the case; the deposition rate calculated for our base conditions in the RDR is 0.23 μm/min, while typical deposition rates reported for channel and barrel reactors (5-7, 10, 58) are in the range 0.04-0.1 μm/min.

Several investigators have compared equilibrium calculations with experimental data to infer details of the SiC deposition mechanism. In one study, Fischman and Petuskey performed equilibrium calculations for the Si—C—Cl—H system (13). In comparing experimental results with the equilibrium data, they observed a marked tendency in the experiments to deposit silicon rather than SiC at C/Si ratios an order of magnitude higher than predicted by thermodynamics. They concluded that gas-phase silicon species are more reactive with substrate surfaces than hydrocarbons and that the rate-limiting step in SiC formation is the deposition of carbon. This conclusion has been confirmed by the surface studies discussed in the section on Chemical Reaction Mechanism. Although the silicon species present in the gas-phase of the Si—C—Cl—H system are different from those present when the initial reactants are SiH_4 and C_3H_8, the gas-phase hydrocarbons are essentially the same (primarily CH_4 and C_2H_2 at equilibrium). Further, the weaker strength of the Si—H bond indicates that these species should be even more likely than Si—Cl

species to deposit rapidly. Thus, our model, predicting that the low efficiency of hydrocarbon surface reactions limits the rate of SiC deposition and that silicon surface deposition is fast, agrees with the conclusions reached by Fischman and Petuskey.

We are aware of two studies that have examined the temperature dependence of the deposition rate over the range of susceptor temperatures typical of cubic silicon carbide growth on silicon; both studies were performed in cold-wall barrel reactors. The results of the two studies are not in complete agreement with each other. Nishino *et al.* found little increase in the growth rate with temperature up to about 1425 K, followed by an exponential increase with an apparent activation energy of 15 kcal/mol over the range 1475-1650 K (6); large error bars on a limited number of data points indicate that the activation energy could be considerably lower than this, however. Powell *et al.* performed studies in a similar reactor (10) and observed little or no dependence on temperature over a limited range of susceptor temperatures (1575-1645 K.) Our results showing little or no change in the deposition rate up to 1600 K followed by exponential growth with an activation energy of 4.9 kcal/mol can thus be considered in reasonable agreement with existing experimental data, given the size of the uncertainties in the data.

Several investigators have examined the effects of varying the concentrations of the reactant gases. Minagawa and Gatos (28) measured the dependence of the SiC deposition rate on the input SiH_4 and C_3H_8 concentrations, using a reactor with geometry similar to the RDR (but with a stationary disk). Their data display trends that are similar to the results presented here, although they were measured at higher temperatures (1873 K). Two studies in horizontal barrel reactors have also been performed. Powell *et al.* (10) found that the silicon carbide growth rate was proportional to the silane concentration and independent of the propane concentration in experiments in which the flow rate of one gas was held constant while the other was varied. Nordquist *et al.* (58) examined the effect of varying the C/Si ratio on the deposition rate; in their experiments, the flow rates of both gases were varied while keeping the (C + Si) atom concentration constant. These two studies appear to contradict our result that the deposition rate is independent of silane and varies linearly with the concentration of propane. However, the data of Nordquist *et al.* may, in fact, be in agreement with our results. If, as indicated by our model, the rate of silicon adsorption by the surface is fast and film growth is limited by the slow deposition of carbon atoms from stable gas-phase species, then variation of the silicon atom fraction (X_{Si}) by adjusting the flow rates of both gases will appear to exhibit a linear dependence on X_{Si} when the variation is actually caused by the adjustment of the propane flow rate. Thus, one cannot conclude from the results of (58) that the rate-controlling step in SiC growth is the addition of silicon to the film surface. One possible source for the disagreement with the results of Powell *et al.* may lie in the fact that the deposition rate varied substantially across the surface of the susceptor in their experiments, being highest at the upstream edge of the wafer and lowest at the downstream edge. The effect of high deposition rates at the upstream edge may be to deplete the boundary layer of silicon species, while the concentrations of hydrocarbon species remain approximately constant, due to the slower hydrocarbon surface chemistry. If the depletion is large enough, a transport dependence on silane concentration could be introduced, thereby masking the effect of the relatively slow hydrocarbon surface reactions. Although the location of the deposition rate measurements on the surface is not stated by Powell *et al.*, we assume that a point near the center of the wafer was used. Measurements close to the leading edge might reveal a different reactant dependence.

Summary

In this paper we have presented a model of the gas-phase and surface chemical reactions leading to the steady-state deposition of silicon carbide. The pyrolysis of the gas-phase reactants, SiH_4 and C_3H_8, is modeled by 83 elementary reactions with rates obtained from the literature. Surface chemistry is included, using 36 elementary reactions whose rates are based on experimentally determined sticking coefficients, surface desorption studies, and theoretical estimates. Our results thus represent the first simulation of a silicon carbide deposition process that includes detailed mechanisms for both the gas-phase and surface reactions. The chemical reaction mechanisms are combined with a previously developed model of a rotating disk reactor in order to predict deposition rates as a function of reactor parameters and to understand the interaction between fluid mechanical effects and the chemistry responsible for film growth.

The results of the model can be summarized by the following picture of SiC deposition under the base conditions adopted here (which are typical of SiC grown on silicon for electronics purposes.) The reactant gases, SiH_4 and C_3H_8, are convected toward the disk by its rotation. At distances less than 1.0 cm above the surface, heat transfer from the hot susceptor causes the gas temperature to rise steeply and the reactants begin to decompose. Propane decomposition yields primarily the stable hydrocarbons CH_4 and C_2H_4, with the production rate of C_2H_4 peaking about 2 mm above the disk, where the gas temperature is about 1350 K. The C_2H_4 decomposes further to produce C_2H_2, although the short residence time at temperatures above 1600 K does not permit complete conversion to C_2H_2. Decomposition of SiH_4 is slower than that of C_3H_8, being inhibited by the hydrogen carrier gas, so its decomposition rate peaks very near the disk surface, where temperatures are highest. Substantial SiH_4 decomposition occurs within 2 mm of the disk, however; SiH_2, Si_2H_2, and Si are the primary decomposition products.

For equal availability of carbon and silicon surface sites, the reactive hydrocarbons in highest concentration, C_2H_4 and C_2H_2, deposit more slowly on the surface than do the decomposition products of SiH_4. This causes the concentration of carbon sites on the surface to be very small. Thus, the deposition rate is limited by the surface chemistry of stable hydrocarbons and is linearly dependent on the input concentration of propane. The slow rates of surface reactions persist even at the highest temperatures examined ($\geq$1800 K), preventing the growth process from becoming completely transport limited.

In examining the temperature dependence of SiC growth in the RDR, it was found that the deposition rate at low temperatures (1500-1600 K) is limited by the C_2H_4 surface reaction. As the temperature of the disk is increased, C_2H_4 near the disk is converted to C_2H_2, so that the primary hydrocarbon responsible for carbon deposition changes from C_2H_4 to C_2H_2. This produces a transition region between the surface reactions of these two molecules for disk temperatures between 1625 K and 1725 K. Above 1725 K, deposition rates no longer increase significantly with temperature due to saturation of the gas-phase C_2H_2 production rate. The model is in reasonable agreement with the limited data available for comparison, although it is clear that the configuration of the reactor (*i.e.*, RDR *vs.* channel reactor) has substantial effects on the gas-phase composition as well as on the fluid mechanics.

It is anticipated that models such as this will be useful in understanding the details of silicon carbide deposition and in optimizing a variety of complex manufacturing processes for producing this material. Extension of this model to the higher temperatures used to deposit alpha-silicon carbide on silicon carbide crystals (above 1873 K) requires that hydrogen etching reactions be included in the surface mechanism. Accurate etching rates as well as additional reactive sticking coefficient data must be obtained at higher temperatures to do this. Further experiments in rotating disk and channel reactors are now required to obtain a more complete understanding of this process.

Acknowledgments

This work was supported by the Department of Energy, Office of Conservation, Office of Industrial Processes Materials Program. The authors would like to thank Dr. Bill Breiland, Dr. Mike Coltrin, Dr. Greg Evans, Dr. Joe Grcar, Dr. Don Hardesty, and Dr. Reggie Mitchell for many illuminating technical discussions. They would also like to ex-

press their great appreciation to Ms. Fran Rupley for her dedicated efforts in code development.

Manuscript received June 25, 1990. This was Paper 616 presented at the Seattle, WA, Meeting of the Society, Oct. 14-19, 1990.

Sandia National Laboratories assisted in meeting the publication costs of this article.

REFERENCES

1. H. J. Kim and R. F. Davis, *J. Appl. Phys.*, **60,** 2897 (1986).
2. K. Minato and K. Fukuda, *J. Nuclear Mat.*, **149,** 233 (1987).
3. J. Federer, *Thin Solid Films*, **40,** 89 (1977).
4. S. Nishino, J. A. Powell, and H. A. Will, *Appl. Phys. Lett.*, **42,** 460 (1983).
5. S. Nishino, H. Suhara, H. Ono, and H. Matsunami, *J. Appl. Phys.*, **61,** 4889 (1987).
6. S. Nishino, Y. Hazuki, H. Matsunami, and T. Tanaka, *This Journal*, **127,** 2674 (1980).
7. P. Liaw and R. F. Davis, *ibid.*, **132,** 642 (1985).
8. A. Suzuki, K. Furukawa, Y. Higashigaki, S. Harada, S. Nakajima, and T. Inoguchi, *J. Crystal Growth*, **70,** 287 (1984).
9. A. Addiamiano and J. A. Sprague, *Appl. Phys. Lett.*, **44,** 525 (1984).
10. J. A. Powell, L. G. Matus, and M. A. Kuczmarski, *This Journal*, **134,** 1558 (1987).
11. A. J. Caputo, W. J. Lackey, and D. P. Stinton, *Ceram. Eng. Sci. Proc.*, **6,** 694 (1985) and references therein.
12. Y. Okabe, J. Hojo, and A. Kato, *J. Less-Common Metals*, **68,** 29 (1979).
13. G. S. Fischman and W. T. Petuskey, *J. Am. Ceram. Soc.*, **68,** 185 (1985).
14. C. D. Stinespring and J. C. Wormhoudt, *J. Crystal Growth*, **87,** 481 (1988).
15. A. I. Kingon, L. J. Lutz, P. Liaw, and R. F. Davis, *J. Am. Ceram. Soc.*, **66,** 558 (1983).
16. J. M. Harris, H. C. Gatos, and A. F. Witt, *This Journal*, **118,** 338 (1971).
17. C. D. Stinespring and J. C. Wormhoudt, *J. Appl. Phys.*, **65,** 1733 (1989).
18. M. E. Coltrin, R. J. Kee, and G. H. Evans, *This Journal*, **136,** 819 (1989).
19. H. Schlichting, "Boundary Layer Theory," 7th ed., McGraw-Hill, Inc., New York (1979).
20. G. Evans and R. Greif, *J. Heat Trans. ASME*, **109,** 928 (1987).
21. G. H. Evans and R. Greif, *Num. Heat Trans.*, **14,** 373 (1988).
22. M. E. Coltrin, Private communication.
23. J. A. Miller and C. F. Melius, Submitted to *Combust. Flame* (1990).
24. C. K. Westbrook and W. J. Pitz, *Comb. Sci. Tech.*, **37,** 117 (1984).
25. M. E. Coltrin and R. J. Kee, Submitted to *J. Crystal Growth* (1990).
26. J. Yoshinobu, H. Tsuda, M. Onchi, and M. Nishijima, *J. Chem. Phys.*, **87,** 7332 (1987).
27. H. Frotzheim, U. Kohler, and H. Lammering, *J. Phys. C.*, **19,** 2767 (1986).
28. S. Minagawa and H. C. Gatos, *Jpn. J. Appl. Phys.*, **10,** 1680 (1971).
29. H. Wagner, R. Butz, U. Backes, and D. Bruchmann, *Solid State Commun.*, **38,** 1155 (1981).
30. H. Frotzheim, H. Lammering, H.-L. Günter, *Phys. Rev. B*, **27,** 2278 (1983).
31. G. Schulze and M. Henzler, *Surf. Sci.*, **124,** 336 (1983).
32. R. J. Buss, P. Ho, W. G. Breiland, and M. J. Coltrin, *J. Appl. Phys.*, **63,** 2808 (1988).
33. L. Muelhoff, W. J. Choyke, M. J. Bozack, and J. T. Yates, *J. Appl. Phys.*, **60,** 2842 (1986).
34. M. E. Coltrin, R. J. Kee, and J. A. Miller, *This Journal*, **133,** 1206 (1986).
35. R. M. Robertson and M. J. Rossi, *J. Chem. Phys.*, **91,** 5037 (1989).
36. P. A. Agrawal, D. L. Thompson, and L. M. Raff, *ibid.*, **91,** 5021 (1989).
37. P. Ho, W. G. Breiland, and R. J. Buss, *ibid.*, **91,** 2627 (1989).
38. I. NoorBatcha, L. M. Raff, and D. L. Thompson, *ibid.*, **81,** 3715 (1984).
39. F. Bozso, J. T. Yates, Jr., W. J. Choyke, and L. Muehloff, *J. Appl. Phys.*, **57,** 2771 (1985).
40. C. J. Mogab and H. J. Leamy, *ibid.*, **45,** 1075 (1974).
41. M. J. Bozack, W. J. Choyke, L. Muehloff, and J. T. Yates, Jr., *ibid.*, **60,** 3750 (1986).
42. M. J. Bozack, P. A. Taylor, W. J. Choyke, and J. T. Yates, Jr., *Surf. Sci.*, **179,** 132 (1987).
43. B. M. Rice, I. NoorBatcha, D. L. Thompson, and L. M. Raff, *J. Chem. Phys.*, **86,** 1608 (1987).
44. J. M. Harris, H. C. Gatos, and A. F. Witt, *This Journal*, **116,** 380 (1969).
45. R. W. Bartlett and R. A. Mueller, in "Silicon Carbide—1968," H. K. Henisch and R. Roy, Editors, Pergamon Press, New York (1969).
46. B. G. Koehler, C. H. Mak, D. A. Arthur, P. A. Coon, and S. M. George, *J. Chem. Phys.*, **89,** 1709 (1988).
47. B. M. Rice, L. M. Raff, and D. L. Thompson, *ibid.*, **88,** 7221 (1988).
48. G. A. Somorjai, "Chemistry in Two Dimensions: Surfaces," Cornell University Press, Ithaca, NY (1981).
49. R. Walsh, *Acc. Chem. Res.*, **14,** 246 (1981).
50. H. C. Abbink, R. M. Broudy, and G. P. McCarthy, *J. Appl. Phys.*, **39,** 4673 (1968).
51. R. Pollard and J. Newman, *This Journal*, **127,** 744 (1980).
52. R. J. Kee, F. M. Rupley, and J. A. Miller, Sandia National Laboratories Report, SAND 89-8009 (1989).
53. G. Dixon-Lewis, *Proc. R. Soc. London, Ser. A*, **307,** 111 (1968).
54. R. J. Kee, G. Dixon-Lewis, J. Warnatz, M. E. Coltrin, and J. A. Miller, Sandia National Laboratories Report, SAND 86-8246 (1986).
55. R. J. Kee, J. F. Grcar, M. D. Smooke, and J. A. Miller, Sandia National Laboratories Report, SAND 85-8240 (1985).
56. J. F. Grcar, R. J. Kee, M. D. Smooke, J. A. Miller, in "Twenty First Symposium (International) on Combustion," The Combustion Institute, Pittsburgh, PA (1986).
57. W. G. Breiland, Private communication (paper in progress).
58. P. E. R. Nordquist, G. Kleiner, M. L. Gipe, and P. H. Klein, *Mater. Lett.*, **8,** 209 (1989).
59. M. E. Coltrin, R. J. Kee, and J. A. Miller, *This Journal*, **131,** 425 (1984).